GPS Solutions (2024) 28:100
https://doi.org/10.1007/s10291-024-01638-2

ORIGINAL ARTICLE

Satellite laser ranging to BeiDou-3 satellites: initial performance and contribution to orbit model improvement

Radosław Zajdel[1] · **Adrian Nowak**[1] · **Krzysztof Sośnica**[1]

Received: 1 September 2023 / Accepted: 1 March 2024

Abstract
In January 2023, the International Laser Ranging Service (ILRS) approved the tracking of 20 additional BeiDou-3 Medium Earth Orbit (BDS-3 MEO) satellites, integrating them into the ILRS tracking network. Before that, only 4 BDS-3 MEO satellites had been tracked. BDS satellites employ highly advanced GNSS components and technological solutions; however, microwave-based orbits still contain systematic errors. Satellite Laser Ranging (SLR) tracking is thus crucial for better identification and understanding of orbit modeling issues. Orbit improvements are necessary to consider BDS in future realizations of terrestrial reference frames, supporting the determination of global geodetic parameters and utilizing them for the co-location of GNSS and SLR in space. In this study, we summarize the first 6 months of SLR tracking 24 BDS-3 MEO satellites. The study indicates that the ILRS network effectively executed the request to track the entire BDS-3 MEO constellation. The number of observations is approximately 1300 and 450 for high- and low-priority BDS-3 satellites, respectively, over the 6 months. More than half of the SLR observations to BDS-3 MEO satellites were provided by 5 out of the 24 laser stations, which actively measured GNSS targets. For 14 out of 24 BDS-3 MEO satellites, the standard deviation of SLR residuals is at the level of 19–20 mm, which is comparable with the quality of the state-of-the-art Galileo orbit solutions. However, the SLR validation of the individual satellites revealed that the BDS-3 MEO constellation consists of more ambiguous groups of satellites than originally reported in the official metadata files distributed by the BDS operators. For 8 BDS-3 satellites, the quality of the orbits is noticeably inferior with a standard deviation of SLR residuals above 100 mm. Therefore, improving orbit modeling for BDS-3 MEO satellites remains an urgent challenge for the GNSS community.

Keywords Satellite laser ranging · ILRS · BeiDou · BDS-3 · Orbit validation · Orbit prediction

Introduction

In January 2023, the International Laser Ranging Service (ILRS; Pearlman et al. 2019) commenced Satellite Laser Ranging (SLR) tracking of 20 additional BeiDou-3 (BDS-3) Medium Earth Orbit (MEO) satellites, which are incorporated into the ILRS tracking network (Pearlman et al. 2019). Up to that point, only 4 BDS-3 MEO satellites had been tracked (Sośnica et al. 2020). The BDS constellation is intriguing for the scientific and GNSS market community, as it employs new concepts and technological solutions, such as innovative navigation signal designs, inter-satellite links, short-message communication capability, and search and rescue services (SAR) (Shi et al. 2020; Xie and Kang 2021; Yang et al. 2021).

SLR tracking of the entire constellation of BDS-3 MEO satellites gives access to a range of new analyses and applications. Firstly, access to SLR observations allows for an independent orbit quality evaluation (Sośnica et al. 2015; Zajdel et al. 2017). SLR provides the accuracy assessment mainly for the radial component (about 96%), because the maximum nadir angles of SLR observations for the GNSS satellites reach up to dozen degrees. However, SLR may also deliver some information about the along-track (2%) and cross-track components (2%). Furthermore, it enables the performance of independent GNSS orbit solutions based solely on laser observations (Pavlis 1995; Bury et al. 2019b), or the combination of both SLR and GNSS observations (Thaller et al. 2011; Hackel et al. 2015; Bury et al. 2020a; Delva et al. 2023). Finally, the SLR observations of GNSS

✉ Radosław Zajdel
radoslaw.zajdel@upwr.edu.pl

[1] Institute of Geodesy and Geoinformatics, Wroclaw University of Environmental and Life Sciences, Grunwaldzka 53, 50-357 Wroclaw, Poland

Published online: 09 April 2024

satellites can be used for determining global geodetic parameters and terrestrial reference frame realization (Sośnica et al. 2018, 2019; Bury et al. 2021; Strugarek et al. 2021).

SLR tracking of GNSS targets

The ILRS collaborates with the International GNSS Service (IGS; Johnston et al. 2017) and other stakeholders to establish a GNSS tracking strategy that aligns with the mission and user requirements (Montenbruck et al. 2017). Some users necessitate increased tracking on specific satellites, while others prefer sparse tracking across the entire GNSS satellite group. Additionally, specific tracking campaigns are requested, such as the study of radiation effects during Earth shadow passages (Steindorfer et al. 2019; Bury et al. 2019b). SLR tracking of GNSS satellites is very challenging because of the low return rate of laser pulses at GNSS heights and a large number of available targets, which results in sparse SLR observations of GNSS satellites. Therefore, ILRS prioritizes the SLR tracking of GNSS to maximize the user needs of orbit validation and co-location in space.

In recent years, the ILRS tracking priority list has undergone occasional changes, leading to variations in the number of prioritized GNSS targets (Zajdel et al. 2023). The current strategy for GNSS tracking by SLR, effective from August 15, 2019, includes the following key points:

- Prioritizing GNSS tracking based on the ILRS standard priority scheme (altitude and inclination), in conjunction with other ILRS satellites.
- Intensively tracking four GNSS satellites per constellation (Galileo, GLONASS, BDS-3) with three sectors (each having at least 2 normal points), spaced widely apart over the pass. These satellites are Galileo-102, -202, -209, -210; beidou3m2, -m3, -m9, and -m10; GLONASS-131, -134, -138, and -139; and QZS-1, -2, -3, and -4. It is important to note that BDS-2 satellites are not included in the ILRS priority list.
- Tracking the remaining GNSS satellites as time permits, with a focus on achieving data diversity among the three constellations.
- Designating special tracking periods for events like satellite eclipses, which are handled separately.

A deviation from the stated assumptions includes the addition of the fifth QZS-1R satellite to the list of priorities and the limited access to GLONASS tracking data from around March 2022, which is associated with the Russian invasion of Ukraine.

Frontiers in BDS-3 orbit modeling

Since the launch of the first BDS-3 satellites in 2017, the orbit modeling was constantly developed by many authors, especially concerning the solar radiation pressure (SRP) modeling. Xu et al. (2019) reported a radial orbit accuracy based on SLR validation of 4–6 cm with a purely empirical modeling of SRP using Empirical CODE Orbit model (ECOM; Arnold et al. 2015). Yan et al. (2019) tested suitability of using different settings of ECOM and developed an adjustable box-wing model for the BDS-3 MEO satellites, proposing its use together with ECOM parameters as an optimal approach to reduce SLR residuals between the lower and higher sun–satellite–earth angle (ε). After release of official metadata information by Test and Assessment Research Center of the China Satellite Navigation Office (CSNO-TARC; CSNO 2019a, b) in December 2019 (see details in Section BDS Constellation Details), Li et al. (2020) utilized this information for SRP and satellite attitude modeling and demonstrated improvements in the orbit overlap compared to the previous studies and entail SLR residuals of 3–6 cm. Duan et al. (2022) extended the work on the use of adjustable box-wing models in the counter-proposal to the use of approximations contained in the metadata and showed improvements by using their a priori box-wing model compared to empirical SRP modeling. The best solution presented by Duan et al. (2022) is characterized by 2.1 cm for orbit misclosures, about 9 cm for 24 h orbit prediction, and 3.7 cm for the standard deviation of SLR residuals. Finally, a recent paper presented by Chen et al. (2023), sheds new light on using the purely empirical approach for BDS-3 SRP modeling, and proves improving the modeling of orbits by adding the fourth- and sixth-order sine terms in the Sun direction when compared to the extended ECOM (Arnold et al. 2015), especially in terms of the orbit misclosures. Based on the analysis of the operational BDS orbit and clock products delivered by IGS multi-GNSS Pilot Project (MGEX; Montenbruck et al. 2017) Analysis Centers (ACs), Steigenberger et al. (2023) concluded that the quality of BDS-3 does not yet reach that of GPS or Galileo. All articles mentioned are limited to assessing the accuracy of orbit modeling based solely on SLR measurements of up to four BDS-3 satellites. However, some indicators describing the precision of the orbits, such as day-to-day orbit misclosures, orbit predictions, and clock stability, indicate differences between the individual satellites. These differences have remained elusive in SLR analysis due to the lack of observations. The previous studies of the individual BDS-3 MEO satellites show that we may distinguish more groups of satellites than reported by CSNO, e.g., based on the patterns in the ECOM parameters (Zajdel et al. 2022) or estimated phase center patterns (Huang et al. 2023). To enhance

our understanding of BDS-3, particularly regarding orbit modeling issues, SLR measurements covering the whole BDS-3 constellation were crucially required for performing the so-called SLR orbit validation to better characterize the BDS-3 constellation and to remove remaining deficiencies in the modeling of orbit dynamics.

Scope of this study

In this study, the dataset of SLR observations to Galileo and BDS satellites was quantitatively and qualitatively evaluated, with the main emphasis on the BDS-3 constellation. The dataset of SLR observations to Galileo satellites is considered a reference that provides an overall picture of the productivity of the ILRS infrastructure in tracking GNSS satellites. Firstly, we introduce the BDS constellation, focusing on the SLR tracking capabilities. Next, the section 'BDS-3 MEO Predictions for ILRS' assesses the availability and quality of the BDS-3 orbit predictions provided for SLR station operators. Section 'BDS tracking' summarizes the ILRS tracking of the GNSS from January till August 2023. Finally, we utilized the SLR dataset to perform the SLR orbit validation and evaluate the quality of the BDS precise orbit products delivered by the Center for Orbit Determination in Europe (CODE), the Wuhan University (WHU), and the European Space Agency (ESA).

BDS constellation details

Following the success of BDS-1 and BDS-2 (Zhao et al. 2022), the BDS-3 constellation began its construction with the launch of the first satellite pair on December 5, 2017. Executing a high-density launch of 30 satellites into the BDS-3 system within three years became possible thanks to the batch development of satellites and the utilization of domestic satellite technologies. BDS-3 construction was completed six months ahead of schedule, setting a new benchmark in the global history of navigation constellation deployment.

The BDS-2 constellation includes five geostationary (GEO), seven inclined geosynchronous (IGSO), and three MEO satellites. Among the 15 BDS-2 satellites, ILRS was involved in supporting only three IGSO satellites, namely C08, C10, C13, and one MEO satellite, C11. The current BDS-3 constellation comprises three GEO, three IGSO, 14 MEO satellites manufactured by the China Academy of Space Technology (CAST; BDS-3M-CAST), and 10 MEO satellites manufactured by the Shanghai Engineering Center for Microsatellites (SECM; BDS-3 M-SECM) of the Chinese Academy of Sciences. Within the BDS-3 constellation, ILRS tracks only the MEO satellites. All 24 BDS-3 MEO satellites are arranged in a three-plane Walker constellation with orbital characteristics including a 55° inclination, a mean altitude of 21,500 km, an orbital period of 12 h and 53 min, and an eccentricity below 0.001. Details aiding the identification of individual BDS-3 MEO satellites by ILRS, IGS, and other stakeholders are provided in Table 1.

CSNO-TARC (CSNO 2019a, b) and Lin et al. (2018) provided essential BDS-3 metadata, including retroreflector offsets, phase center offsets, attitude law, approximate spacecraft mass, dimensions, and a subset of optical parameters. However, the accuracy of SRP modeling is constrained by the absence of information on the reflection and diffusion properties of satellite surfaces and solar panels (Li et al. 2020). Access to only approximate metadata values further limits the precision of the modeling. Past studies have indicated that utilizing metadata from official BDS sources does not offer as many advantages for orbit modeling or for using BDS-3 to establish the reference frame scale, as observed with the release of Galileo metadata (GSA 2017; Bury et al. 2019a, 2020b; Li et al. 2020; Duan et al. 2022). Furthermore, Zajdel et al. (2022) indicated that the patterns visible in the estimated accelerations of the Empirical CODE Orbit Model (ECOM; Arnold et al. 2015) revealed up to ten different groups of satellites among the BDS-3 constellation. These clusters share similar patterns in their estimated ECOM parameters. The official metadata (CSNO 2019a) only provide a single set of parameters for all the CAST satellites, but beyond this, we are aware of four CAST satellites outfitted with SAR antennas—specifically, C32/C33 (beidou3m13/m14) and C45/C46 (beidou3m23/m24), as detailed by (Li et al. 2021). As the presence of SAR antenna, which protrude beyond the satellite body, is not provided in the satellite a priori model based on the metadata, it is reasonable to anticipate unique ECOM signatures. Within the SECM satellite group, metadata differentiate between SECM-A and SECM-B satellites. These two types possess differing dimensions according to CSNO metadata records. However, the contrast primarily lies in the Y cross-sectional area, whereas the X and Z dimensions remain nearly identical. Furthermore, BDS-3 M-SECM satellites exhibit a distinct stretching direction compared to BDS-3M-CAST satellites.

In terms of laser ranging capability, both SECM and CAST satellites are equipped with a planar laser retroreflector array (LRA). The LRAs for the BDS-3 M-SECM satellites are produced by the Shanghai Observatory (SHA). These arrays consist of 42 circular corner cubes, each with a diameter of 33 mm, as reported by (Zhang et al. 2014). This same LRA module was installed on the previous generation of the BDS-2 satellites. Regarding the BDS-3M-CAST satellites, the LRAs are designed by the North China Research Institute of Electro-Optic (NCRIEO). These LRAs comprise 38 circular corner cubes, each with a diameter of 33 mm. For further details, we refer readers to the IGS Satellite Metadata File, which

Table 1 Identification of the BDS-3 MEO satellites

ILRS name	BDS-SVN	NORAD ID	COSPAR	SVN	PRN	Launch date	Type
beidou3m1	MEO-1	43,001	2017-069A	C201	C19	05.11.2017	BDS-3M-CAST
beidou3m2	MEO-2	43,002	2017-069B	C202	C20	05.11.2017	BDS-3M-CAST
beidou3m3	MEO-3	43,208	2018-018B	C206	C21	12.02.2018	BDS-3M-CAST
beidou3m4	MEO-4	43,207	2018-018A	C205	C22	12.02.2018	BDS-3M-CAST
beidou3m5	MEO-5	43,581	2018-062A	C209	C23	29.07.2018	BDS-3M-CAST
beidou3m6	MEO-6	43,582	2018-062B	C210	C24	29.07.2018	BDS-3M-CAST
beidou3m11	MEO-11	43,603	2018-067B	C212	C25	24.08.2018	BDS-3 M-SECM-A
beidou3m12	MEO-12	43,602	2018-067A	C211	C26	24.08.2018	BDS-3 M-SECM-A
beidou3m7	MEO-7	43,107	2018-003A	C203	C27	11.01.2018	BDS-3 M-SECM-A
beidou3m8	MEO-8	43,108	2018-003B	C204	C28	11.01.2018	BDS-3 M-SECM-A
beidou3m9	MEO-9	43,245	2018-029A	C207	C29	29.03.2018	BDS-3 M-SECM-A
beidou3m10	MEO-10	43,246	2018-029B	C208	C30	29.03.2018	BDS-3 M-SECM-A
beidou3m13	MEO-13	43,622	2018-072A	C213	C32	19.09.2018	BDS-3M-CAST
beidou3m14	MEO-14	43,623	2018-072B	C214	C33	19.09.2018	BDS-3M-CAST
beidou3m15	MEO-15	43,648	2018-078B	C216	C34	15.10.2018	BDS-3 M-SECM-A
beidou3m16	MEO-16	43,647	2018-078A	C215	C35	15.10.2018	BDS-3 M-SECM-A
beidou3m17	MEO-17	43,706	2018-093A	C218	C36	18.11.2018	BDS-3M-CAST
beidou3m18	MEO-18	43,707	2018-093B	C219	C37	18.11.2018	BDS-3M-CAST
beidou3m19	MEO-19	44,864	2019-090A	C227	C41	16.12.2019	BDS-3M-CAST
beidou3m20	MEO-20	44,865	2019-090B	C228	C42	16.12.2019	BDS-3M-CAST
beidou3m21	MEO-21	44,794	2019-078B	C226	C43	23.11.2019	BDS-3 M-SECM-B
beidou3m22	MEO-22	44,793	2019-078A	C225	C44	23.11.2019	BDS-3 M-SECM-B
beidou3m23	MEO-23	44,543	2019-061B	C223	C45	22.09.2019	BDS-3M-CAST
beidou3m24	MEO-24	44,542	2019-061A	C222	C46	22.09.2019	BDS-3M-CAST

contains the most up-to-date information and references (Steigenberger and Montenbruck 2022).

BDS-3 predictions for ILRS

Orbit predictions are essential for SLR stations to effectively track satellites. For the BDS-3 MEO satellites, these predictions are exclusively supplied by the Shanghai Observatory (SHA). Figure 1 illustrates the availability of new orbit prediction files on the Crustal Dynamics Data Information System (Noll 2010). The average time between successive releases of these new satellite prediction files is approximately 3 days, with occasional intervals of 5 to 10 days. SHA's orbit predictions extend for 9 consecutive days following each release. However, it is important to note that the accuracy of orbit predictions decreases exponentially as the days progress.

Interestingly, SHA stopped providing predictions for beidou3m7 (C27) and beidou3m8 (C28) at the start of March. However, there is no information available about the malfunction of these satellites, and the post-processed MGEX orbit products are being provided continuously by the IGS ACs (Steigenberger et al. 2023). In February 2023, several SLR stations failed to get returns from either satellite despite

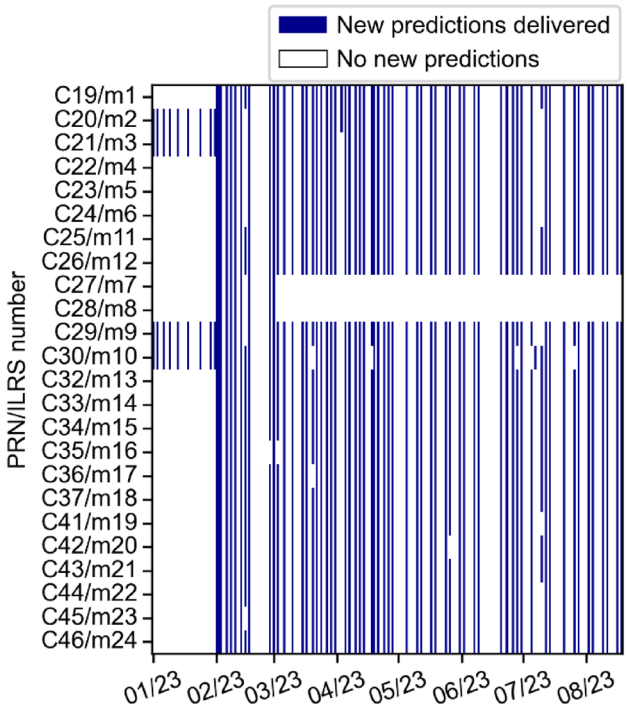

Fig. 1 Availability of orbit prediction files delivered by SHA for BDS-3 MEO satellites for each day in 2023. The satellites are identified by BDS-3 PRN and ILRS numbers (see Table 1)

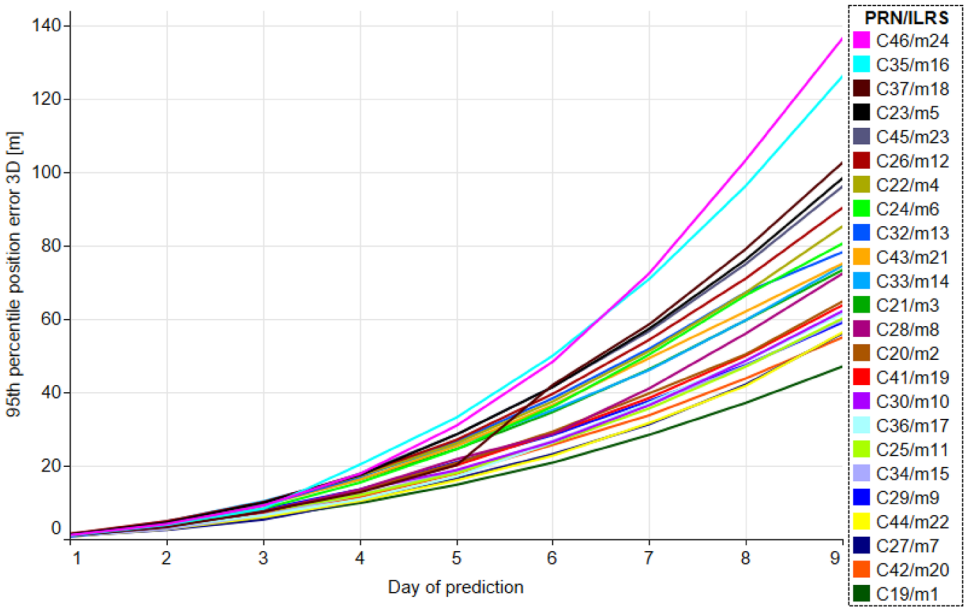

Fig. 2 Degradation of the orbit prediction quality for all the BDS-3 MEO satellites. The 95th percentile for each day of prediction is shown. The legend is sorted by the error in the last day of prediction.

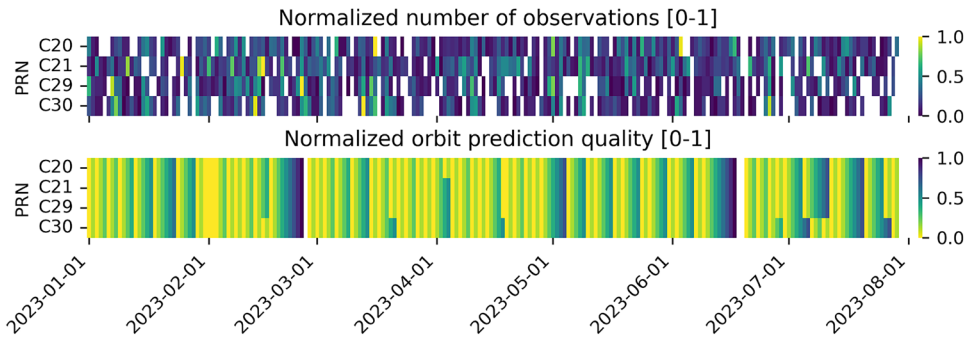

Fig. 3 The number of observations provided for high-priority BDS-3 satellites (top) and prediction quality (bottom) normalized to the range from 0 to 1

good quality of orbit predictions. Of the potential reasons for the problem of getting observations to these satellites, the most likely seems to be an obstruction of the LRA by some structural element, or an attitude problems. As a consequence of the failure of the observation acquisition, ILRS removed them from the list of targets.[1]

Figure 2 illustrates the degradation of orbit prediction quality over time for all BDS-3 MEO satellites. The orbit prediction quality is determined by the epoch-wise differences between the predicted satellite positions and the reference orbit. For this analysis, we utilized the reference COD0MGXFIN orbits (Prange et al. 2020), which exhibit an approximate accuracy of 5 cm, as confirmed through the independent SLR validation dataset (refer to the next Section). The 95th percentile of the predicted satellite position 3D error varies among individual satellites, measuring between 1 to 5 m, 10 to 25 m, and 32 to 118 m after 1, 5, and 9 days of prediction, respectively. When considering the availability of new prediction files (as shown in Fig. 1), data from consecutive days, specifically 5 to 9 days, must also be employed by SLR station operators. Furthermore, comparing these results to the prediction quality offered for other GNSS, such as Galileo (Najder and Sośnica 2021), we may anticipate achieving meter-level accuracy in a 5-day prediction, assuming that the orbit modeling strategy is adjusted per GNSS constellation and satellite type, especially concerning the handling of SRP (Nowak et al. 2023). Figure 3 illustrates the number of SLR observations provided for high-priority BDS-3 satellites (top) and prediction quality (bottom) normalized to the range from 0 to 1. One should note that there is no linear correlation between prediction quality and the number of observations, suggesting that the existing prediction quality is sufficient for the ILRS purposes. Even in cases where SHA does not provide a new predictions file (end of February and mid of June), SLR observations remain accessible. It can therefore be concluded that SLR stations utilize in-house orbit extrapolation in the absence of new predictions.

[1] https://ilrs.gsfc.nasa.gov/missions/satellite_missions/current_missions/index.html

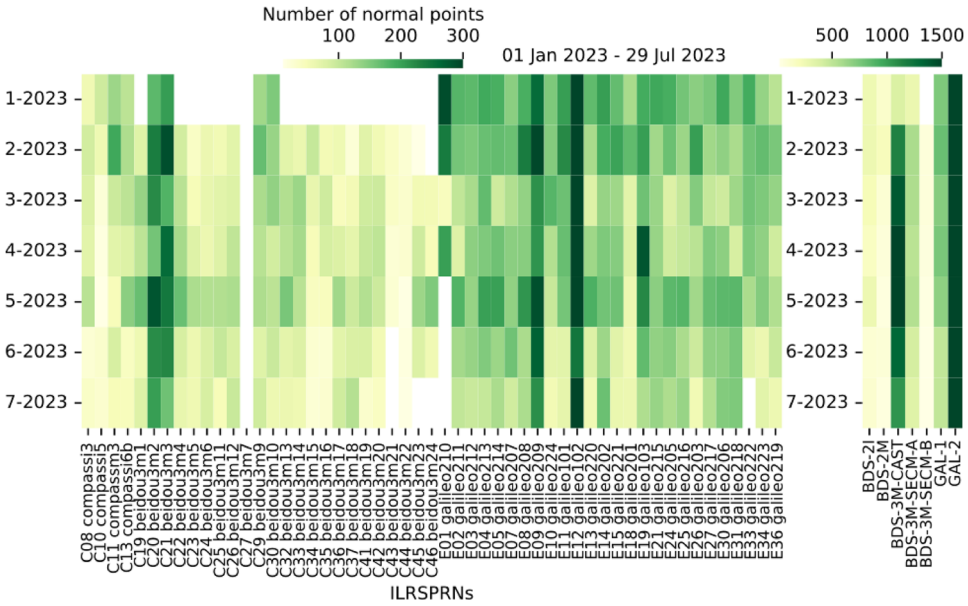

Fig. 4 Number of SLR normal points delivered for individual BDS and Galileo satellites in each month from January to July 2023

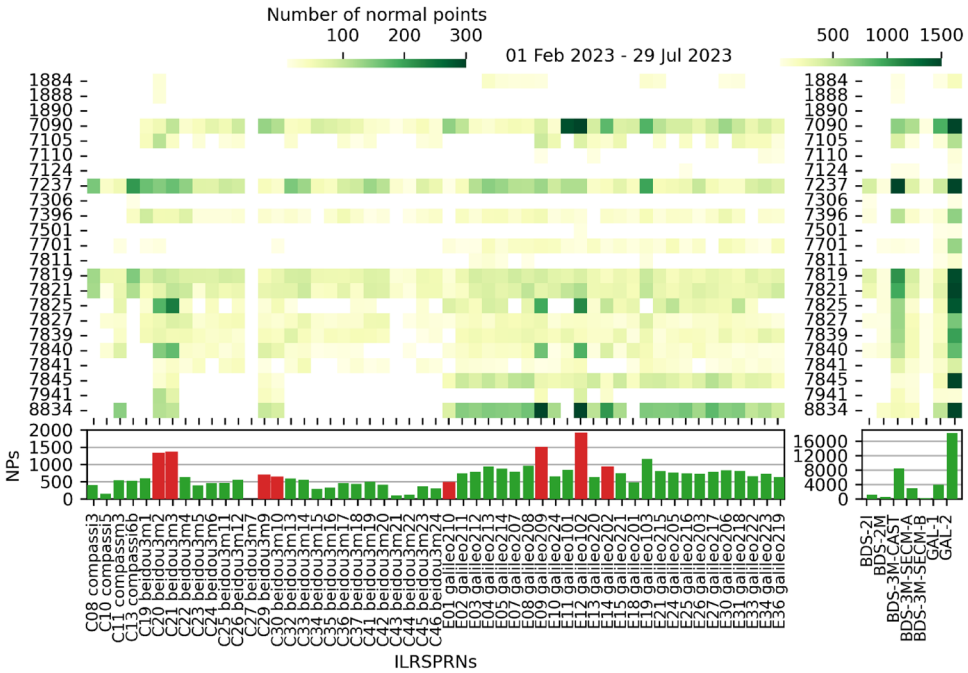

Fig. 5 Number of SLR normal points delivered by ILRS stations for individual BDS and Galileo satellites between January and August 2023. Individual satellites are identified by PRN and ILRS number (see Table 1)

BDS tracking performance

Figure 4 illustrates the number of normal points delivered each month from the beginning of January to the end of July 2023 by all stations for individual BDS-2, BDS-3, and Galileo satellites (left column), along with groupings by satellite types (right column). For the purpose of the SLR validation of GNSS orbits, it is not always essential to attain equal coverage of observations for all satellites. Generally, the quality of orbit modeling remains uniform within satellites of the same type. An exception arises in cases of misbehaving satellites (Dach et al. 2019; Bury et al. 2022), which need identification and individual treatment. Nevertheless, the number of observations per satellite type serves as an indicator of the information available for assessing the orbit modeling of that specific satellite type. Figure 5 complements Fig. 4 by depicting the number of SLR normal points delivered by individual ILRS stations for the same set of satellites. In Fig. 5, satellites listed in the ILRS mission priorities for 2023 are highlighted in red in the bottom bar plots.

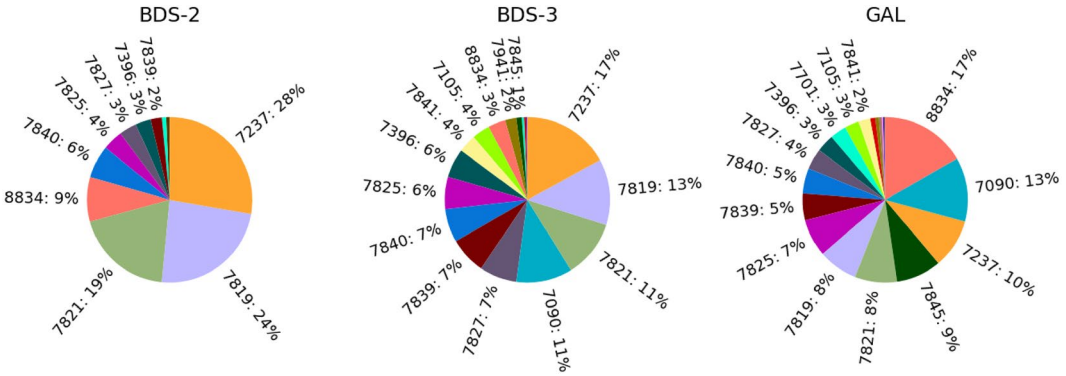

Fig. 6 Participation of the ILRS stations in GNSS tracking grouped by satellite systems

Firstly, let us get an insight on what is the impact of the new BDS tracking plan on the ILRS network performance. Station operators had to allocate their resources to track 20 additional targets. Using January and March 2023 as an example (refer to Fig. 1), we looked at how the station's efficiency in GNSS tracking has changed. Comparing the two months, it can be seen that the number of observations to Galileo fell by around 30%, with the number of observations recorded in total for both Galileo and BDS-3 falling by only 8%. So, we see that part of the station's commitment to tracking Galileo has been redirected toward new objectives of BDS-3.

For BDS-3, the four highest priority satellites receive indeed the most robust support. However, it is worth noting that beidou3m2/m3 satellites have approximately twice as many observations as beidou3m9/m10. Notably, the number of observations for m9 and m10 satellites is only 1.3 times higher than for the remaining BDS-3 satellites. The average number of normal points during the analyzed period is approximately 1300, 650, and 400 for beidou3m2/m3, beidou3m9/m10, and the remaining BDS-3 satellites, respectively. Interestingly, there are no SLR observations for the beidou3m7/m8 satellites. This absence is due to the lack of orbit predictions for these satellites, which were only available for one month from February 1st to March 1st.

For Galileo, two out of four high-priority Galileo satellites, i.e., galileo209 and 102, are indeed the most frequently tracked by the ILRS network with more than 1500 normal points recorded in 6 months. On the other hand, the other two high-priority satellites are similarly (E14 galileo202) or even worse (E01 galileo210) supported against the whole Galileo pool. On average, 800 normal points were delivered for the remaining Galileo satellites. Comparing the number of normal points for the BDS-3 and Galileo satellites, the stations provide almost two times more observations for Galileo than for the BDS-3 satellites for the non-ILRS priority satellites.

Figure 6 and Table 2 display the involvement of individual stations in tracking GNSS satellite types and the overall systems. Over half of the normal points to BDS-3 MEO satellites were contributed by five out of the 24 laser stations, which actively measured GNSS targets: 7237 (Changchun, 17%), 7819 (Kunming, 13%), 7821 (Shanghai, 11%), 7090 (Yarragadee, 11%), and 7827 (Wettzell, 7%). During the same period, the Galileo constellation was predominantly supported by: 8834 (Wettzell, 17%), 7090 (Yarragadee, 13%), 7237 (Changchun, 10%), 7845 (Grasse, 9%), 7819 (Kunming, 8%), and 7821 (Shanghai, 8%). One should also note a discernible prioritization of tracking stations.

The Chinese and Australian stations, namely 7819, 7821, 7237, 7825, and 7090, demonstrate high productivity by tracking all potential GNSS targets. The European stations are divided into two distinct groups. Both groups predominantly focus on the domestic Galileo constellation. However, for other systems such as BDS, stations 7845, 7941, and 8834 exclusively observe high-priority satellites. In the second group, stations 7839, 7840, and 7841 also support the remaining satellites, albeit with lower intensity.

SLR validation of the BDS final orbits

In this study, we assessed the quality of the Galileo and BDS precise orbit products provided by the CODE (COD-0MGXFIN; COD; Prange et al. 2020), WHU (WUM-0MGXFIN; WUM; Guo et al. 2016), and ESA (ESA-0MGNFIN; ESA; Enderle et al. 2023) between February and August 2023. In accordance with the product nomenclature, all these products fall under the category of IGS final products and are released with latencies ranging from four days to three weeks. Steigenberger et al. (2023) provide a comprehensive discussion of the BDS-3 orbit and clock processing scheme implemented by COD and WUM for their MGEX products (refer to Table 2), while the specifics of the ESA products are detailed by Enderle et al. (2023).

Table 2 Percentage share of normal points delivered for individual groups of GNSS satellites by ILRS stations

No	Place	Satellite type							Constellation		
		BDS-2 IGSO	BDS-2 MEO	BDS-3 CAST	BDS-3 SECM	GAL-FOC	GAL-FOCe	GAL-IOV	BDS-2	BDS-3	GAL
1884	Riga, Latvia	0	0	0	0	1	0	1	0	0	0
1888	Svetloe, Russia	0	0	0	0	0	0	0	0	0	0
1890	Badary, Russia	0	0	0	0	0	0	0	0	0	0
7090	Yarragadee, Australia	0	0	8	19	10	18	23	0	11	13
7105	Greenbelt, USA	0	0	4	1	3	2	2	0	4	3
7110	Monument Peak, USA	0	0	0	0	0	0	0	0	0	0
7124	Tahiti, French Polynesia	0	0	0	0	0	0	0	0	0	0
7237	Changchun, China	36	10	19	12	10	6	11	34	17	10
7306	Tsukuba, Japan	1	0	0	0	0	0	0	0	0	0
7396	Wuhan, China	4	0	6	4	4	4	2	0	6	4
7501	Hartebeesthoek, South Africa	0	0	0	0	0	0	0	0	0	0
7701	Izaña, Spain	0	3	0	0	4	2	2	0	0	3
7811	Borowiec, Poland	0	0	0	0	1	0	0	0	0	0
7819	Kunming, China	30	11	13	14	8	6	6	30	13	8
7821	Shanghai, China	23	11	11	12	8	8	8	24	11	8
7825	Mt Stromlo, Australia	0	12	7	3	7	12	6	0	6	8
7827	Wettzell, Germany	3	5	7	7	4	4	4	4	7	4
7839	Graz, Austria	0	7	7	7	6	4	4	0	7	5
7840	Herstmonceux, UK	3	14	6	7	4	10	7	8	7	5
7841	Potsdam, Germany	0	0	4	3	2	2	3	0	4	2
7845	Grasse, France	0	0	1	2	10	5	6	0	1	9
7941	Matera, Italy	0	0	2	2	0	2	2	0	2	1
8834	Wettzell, Germany	0	27	3	6	18	15	13	0	3	17

The most crucial distinctions in the processing features implemented by the ACs can be observed in the parametrization of the solutions, including satellite clocks, troposphere parameters, and station coordinates. Additionally, differences exist in the strategies employed for SRP modeling.

In the case of CODE, SRP modeling utilizes the 7-parameter extended ECOM model (Arnold et al. 2015). This involves constant coefficients in the D, Y, and B directions, along with once-per-revolution sine and cosine terms in the B direction (B1S, B1C), and twice-per-revolution sine and cosine terms in the D direction (D2S, D2C). Here, D represents the Sun–satellite axis, Y is the axis along solar panels, and B is perpendicular to D and Y, completing the right-handed orthogonal frame. Conversely, WHU employs an empirically adjusted box-wing model (Wang 2019), supported by the 5-parameter ECOM model (Springer et al. 1999), including D0, Y0, B0, B1C, and B1S. WHU's approach also incorporates the estimation of empirical constant acceleration in the along-track direction. In the case of the ESA solution, the coefficients for the box-wing model are derived from an internal study and are not publicly available. Furthermore, ESA's orbit modeling approach makes use of 5 parameters (D0, Y0, B0, B1C, and B1S) of the ECOM model (Springer et al. 1999), along with once-per-revolution and constant empirical parameters in the along-track direction.

The SLR orbit validation was conducted using the Bernese GNSS Software 5.4 (Dach et al. 2015). Residuals from SLR observations (later referred to as SLR residuals) were computed by calculating the differences between laser measurements and the microwave-derived positions of GNSS satellites. The coordinates of SLR stations were held constant in the SLRF2020 (2023) reference frame, without accounting for seasonal station coordinate variations. The positions of satellites were provided in the IGS20 reference frame and sampled at 5-min intervals. Both IGS20 and SLRF2020 are consistent in rotation, origin, and scale with ITRF2020 (Altamimi et al. 2023).

The IGS20 ANTEX file, containing satellite antenna models, was employed by the CODE and WHU ACs during their orbit processing, inferring from the header of the SP3 files. The radial phase center offsets (z-PCOs) for GPS, GLONASS, and Galileo satellites within the IGS20 ANTEX file were adjusted to match the ITRF2020 scale. These adjusted values were determined from a series of z-PCO estimates derived from daily IGS repro3 solutions of 9 ACs. Unified corrections were calculated and applied to the calibrated z-PCOs of all Galileo satellites, except E102, as provided by the European GNSS Agency (GSA 2017). Satellite-specific z-PCOs were determined for all remaining satellites. Concerning BDS-3 satellites, the IGS20.atx file incorporates band-specific calibrations published by CSNO. Notably, while the terrestrial scale indicated by the z-PCOs of GPS, GLONASS, and Galileo satellites in the IGS20 ANTEX file matches the ITRF2020 scale at the epoch of 2015.0, a gradual deviation from the ITRF2020 scale occurs at an approximate rate of + 0.1 mm per year (Steigenberger and Montenbruck 2023). Unfortunately, this is not addressed in the current ANTEX format. For BDS, the z-PCO is not aligned with the ITRF2020 scale, resulting in an anticipated systematic offset in the SLR residuals.

ESA orbit determination strategy employs distinct PCO values for Galileo and BDS satellites than those included in the IGS20 ANTEX file (Enderle et al. 15). For Galileo, official PCO values from the European GNSS Service Centre were utilized, while ESA estimates were used for BDS-3. Unfortunately, these files are not publicly available, making it challenging to assess their inter-AC inconsistency arising from different models.

To synchronize with SLR measurement times, satellite discrete Earth-fixed positions sampled with 5-min intervals were interpolated using the orbit fit based on orbit dynamics. For the latter, we used 7-parameter extended ECOM model (Arnold et al. 2015) together with a priori box-wing model based on the official metadata (Li et al. 2020). Transformations between Earth-fixed and inertial frames were accomplished using the Earth orientation parameter series distributed by ACs together with orbits. LRA offset values provided by CSNO are incorporated to take into account the difference between the LRA, i.e., the reference point of the SLR observations and the spacecraft's center of mass, to which the orbit refers to. The models for station displacement, which encompass effects such as solid Earth tides, ocean tidal loading (FES2014b; Lyard et al. 2021), and mean pole definition, adhere to the standards of the International Earth Rotation and Reference System Service (IERS) Conventions 2010 (Petit and Luzum 2010, version 1.3.0). Orbit modeling inconsistencies between orbit fit and AC-specific processing strategy were mitigated by estimating pseudo-stochastic pulses every hour in the orbit radial, along-track, and cross-track directions. Figure 7 provides statistics on the quality of the orbit fit in the radial direction, which is directly relevant for SLR validation. Specifically focusing on BDS-3, the fit quality is at the level of approximately single millimeters, with the median difference closely approaching 0. The COD and ESA orbits are more accurately reconstructed than WHU's WUM, although this discrepancy arises from processing strategy inconsistencies between the original approach employed by the ACs and the reconstruction method used in this study. These values should be considered as interpolation errors when interpreting SLR orbit validation results.

We utilize a two-phase process to screen SLR data residuals. In the initial stage, we exclude only the gross residuals that surpass the 200 mm threshold. Subsequently, the z-score

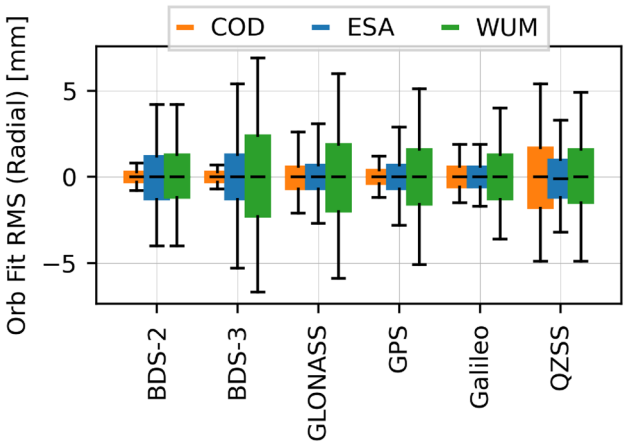

Fig. 7 Orbit fit quality in the radial orbit direction. The box ranges from 1st to the 3rd quartile. A horizontal line inside the box reflects the median. The whiskers go from 5 to 95th percentile

method for rejecting outliers is applied for SLR residuals related to each station–satellite pair. The z-score method in outlier detection calculates the standard score for each data point, representing its deviation from the mean in terms of standard deviations, and outliers are identified based on a predetermined threshold. The SLR residuals are rejected if the z-score of a data point is more than 3.

Results of the BDS orbit validation

Figure 8 shows box plots of SLR residuals for different satellite groups. Table 3 sums up the statistics of SLR residuals for different satellite types. The mean offset of SLR residuals for individual satellites varies within the range of −50–50 mm. When considering only the mean offset, the BDS-3M-CAST satellites can be categorized into three groups: C32/C33 as BDS-3 CAST SAR-A, C45/C46 as BDS-3 CAST SAR-B, and all other CAST satellites as BDS-3M-CAST. Duan et al. (2022) have reported potential satellite construction differences for the C36/C37 pair, where empirically adjusted box-wing parameters differed from the other BDS-3M-CAST satellites (C19-C24). This observation was further confirmed by Zajdel et al. (2022) through analysis of ECOM coefficients estimated in the orbit solutions. In our analyses, the C36/C37 satellites are indicated with an asterisk suffix (BDS-3M-CAST*). The mean offset for BDS-3M-CAST satellites generally falls within the range of 30–40 mm. However, the pair C32/C33 (BDS-3M-CAST SAR-A) exhibits a distinct offset of approximately −20 mm. Notably, the offset for this group is more akin to the BDS-3 SECM-A satellites, which also feature SAR instruments, than to the remaining BDS-3M-CAST satellites. Within the BDS-3-SECM-A satellites, we additionally distinguish the pair of C34/C35 satellites. The variations between the ACs are more pronounced in this pair compared to the remaining BDS-3M-SECM-A satellites, and they are denoted with an asterisk suffix (BDS-3M-SECM-A*). The variations in the mean SLR offset can be attributed to specific modeling options related to antenna thrust, Earth's albedo, or SRP modeling, as discussed in studies by Bury et al. (2019a) and Prange et al. (2020). For the BDS-3 satellites, insights from orbit modeling studies on GIOVE-B by Steigenberger et al. (2015) reveal that addressing the shadow cast by the LRA support plate can reduce the SLR bias by approximately 10 cm. A comprehensive understanding of spacecraft

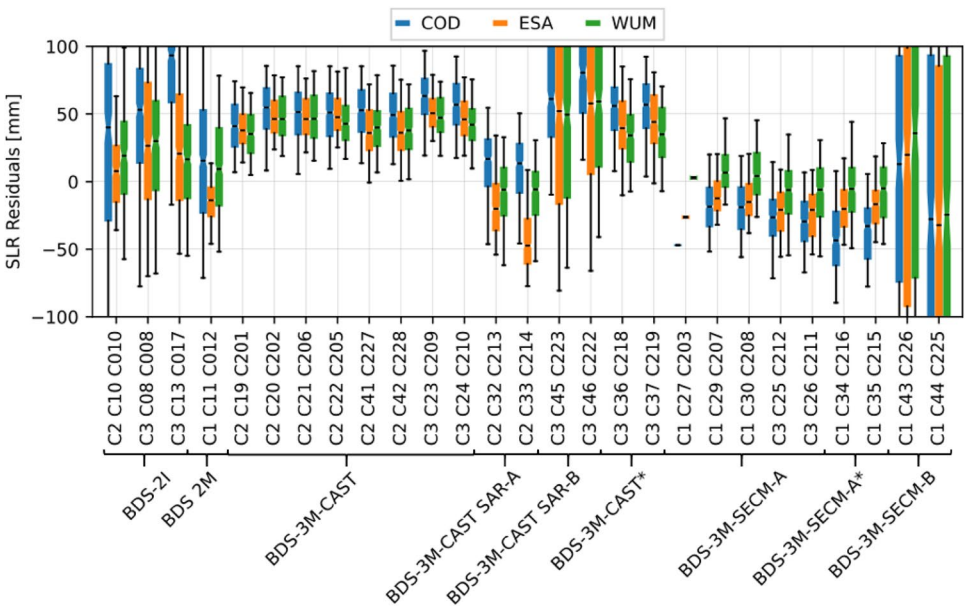

Fig. 8 GNSS orbit validation based on SLR observations for individual satellites. The box ranges from 1st to the 3rd quartile. A vertical line inside the box reflects the median. The whiskers go from 5 to 95th percentile. The individual satellites are labelled by sequentially: type, orbital plane, PRN number, and SVN number

Table 3 Statistics of SLR residuals for different satellite types

		BDS-2I	BDS-2 M	BDS-3M-CAST	BDS-3M-CAST SAR-A	BDS-3M-CAST SAR-B	BDS-3M-CAST*	BDS-3 M-SECM-A	BDS-3 M-SECM-A*	BDS-3 M-SECM-B
COD	Mean	56	18	51	11	81	54	−22	−39	−2
ESA		21	−15	46	−30	58	42	−16	−18	−3
WUM		21	11	45	−8	58	34	2	−6	5
COD	STD	71	59	**24**	**30**	56	**27**	**24**	**28**	110
ESA		51	**18**	**19**	**29**	82	**27**	**20**	**20**	112
WUM		52	39	**21**	**28**	74	**26**	**26**	**26**	114
COD	RMS	90	61	56	32	99	61	33	48	110
ESA		55	**24**	50	42	101	49	**25**	**27**	112
WUM		56	40	49	**29**	94	42	**26**	**27**	114

All values in millimeters. STD—standard deviation. RMS—root mean square. STD and RMS values below 30 mm are bolded

characteristics is crucial to assess similar effects for BDS-3 satellites.

The standard deviation (STD) of SLR residuals is largely consistent among the majority of BDS-3M-CAST and BDS-3M-SECM satellites, ranging from 20 to 28 mm. Exceptions include BDS-3M-CAST SAR-B (C45/C46) and BDS-3M-SECM-B (C43/C44), which exhibit substantially higher STD of up to 100 mm. The products provided by different ACs show consistency in terms of general patterns and the categorization of satellite groups. However, the mean offsets differ systematically for each group, which is particularly noticeable for the BDS-3M-SECM satellites, where offsets vary by up to 15 mm. Differences in mean offsets among satellites may stem from the cumulative effect of errors originating from factors such as uncertainty in LRA offset as provided by CSNO, scale inconsistency between satellite antenna z-PCO and the reference frame, errors in satellite antenna z-PCO values (Zajdel et al. 2022; Huang et al. 2023), different antenna thrust values, inaccurate satellite surface properties used for orbit models, and station–satellite-dependent range bias, which may not have been appropriately addressed (Rodríguez et al. 2019; Strugarek et al. 2021; Zajdel et al. 2023).

Signatures in SLR residuals

The purpose of the following analysis is to reveal observable patterns within distinctive geometric configurations involving the Sun, Earth, and satellites. The overarching objective is to examine the advantages and limitations inherent in the solutions provided by different ACs, as well as to identify distinct types of satellite groups within the constellation, thereby validating the conclusions drawn from the previous analysis. This investigation will entail analyzing the SLR residuals, with a particular emphasis on their fluctuations as a function of three key factors: the Sun elevation angle above the orbital plane (absolute value of β), the elongation angle between the satellite and the Sun (referred to as ε), and the latitude of the satellite within the Sun–Earth–satellite configuration (Δu) (refer to Fig. 9). The dataset of SLR residuals covers almost exactly a half of the BDS-3 draconitic year, which is approximately 360 days. That allows for the orbit quality assessment based on the full range from 0 to the maximum β angle. The maximum β angles for the particular BDS-3 planes are about 34°, 63°, and 74° for C1, C2, and C2 orbital planes, respectively. For the next analyses, the mean offset was removed individually for each satellite solution to ensure that they do not obscure the patterns of interest.

Figure 10 depicts the SLR residuals plotted as functions of the Sun elevation angle above the orbital plane (absolute value of β) and the satellite argument of latitude relative to the latitude of the Sun (Δu) across various AC solutions. Although we supplied a dataset encompassing the entire range of Δu and β, the graphs exhibit missing data points.

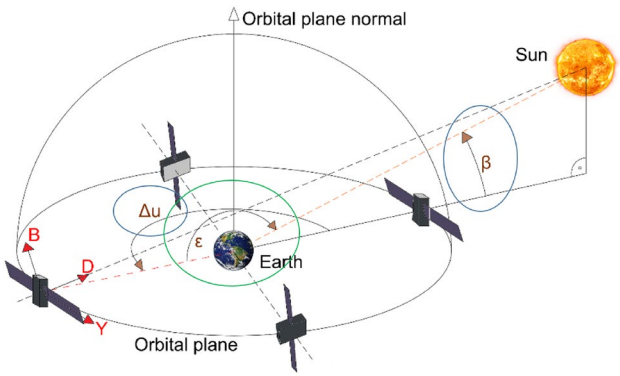

Fig. 9 Sun–Earth–satellite geometry. β—elevation of the Sun above the orbital plane; Δu—satellite argument of latitude with respect to the latitude of the Sun; ε—the satellite elongation angle with respect to the position of the Sun. The vectors of D,Y,B explain the sun-oriented frame as used in ECOM model. After Zajdel et al. (55)

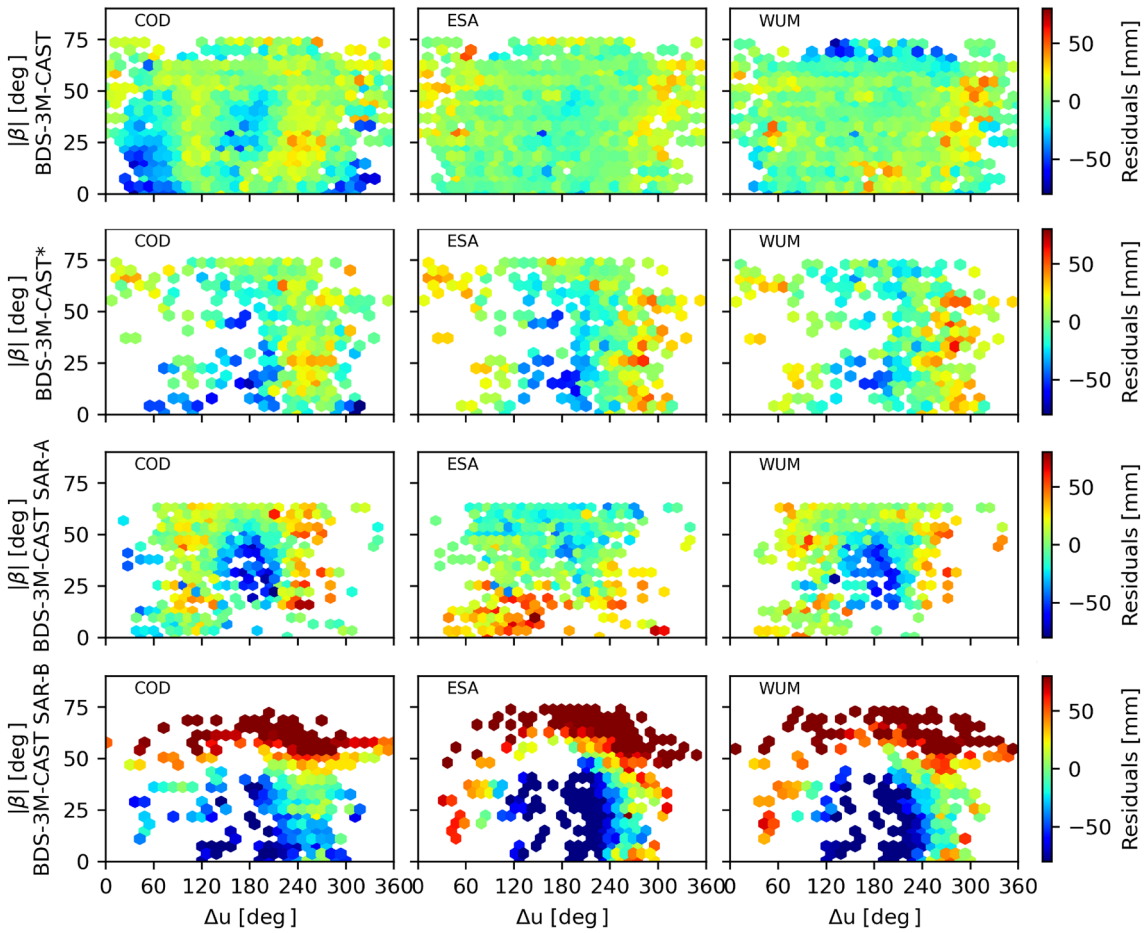

Fig. 10 SLR residuals as a function of the Sun elevation angle above the orbital plane (absolute value of β) and the satellite argument of latitude with respect to the latitude of the Sun (Δu) based on the individual AC solutions for different subgroups within BDS-3 MEO satellites manufactured by CAST. The mean value of SLR residuals in each grid cell is depicted

This is attributed to the limited efficiency of the stations in furnishing SLR observations, with an insufficient number available for a specific group. Another contributing factor to this shortfall is the inherent limitation of the SLR technique, which restricts its ability to track satellites near Δu close to 0/360°. Within the primary group of BDS-3M-CAST satellites, the COD products reveal a distinct pattern in SLR residuals shifted toward negative values for Δu values close to 0/360°. These patterns are not discernible in either ESA or WUM orbit solutions. Both ESA and WUM as opposed to COD employ a box-wing model in their solution, which seems to mitigate the orbit modeling issues for this group to a significant extent. This is confirmed by a similar analysis done for Galileo; similar pattern is particularly prominent for the solutions utilizing only solely empirical approaches handling for SRP (e.g., using ECOM), but largely disappears when employing the a priori box-wing model together with empirical parameters (Zajdel et al. 2023).

Conversely, for WUM solutions, substantial negative residuals exceeding −50 mm manifest for maximal $|\beta|$ angles (above 70°). In scenarios with high β angles, the orbital direction B of the ECOM model aligns with the radial direction directly measured by SLR (Bury et al. 2020a). Regarding the C36/C37 satellites, categorized as BDS-3M-CAST*, SLR residuals appear more negative for Δu values close to 180°. This same pattern of SLR residuals is evident for BDS-3M-SAR-A satellites, except for the orbit solution provided by ESA, where the negative SLR residuals are substituted with visibly higher residuals at $|\beta|$ angles below 25°.

Finally, the orbit modeling approach employed by the ACs for the last group, encompassing satellites C45/C46 (BDS-3M-CAST SAR-B), requires modification to achieve accuracy comparable to that of the other satellites.

Figure 11 illustrates the relationships between SLR residuals and satellite elongation angles relative to the Sun. In this analysis, the orbit modeling quality for a specific satellite type can be quantified by the coefficient value of the linear correlation between SLR residuals and the elongation angle. The linear correlation is the smallest for the BDS-3M-CAST satellites, ranging from 0.001 to approximately

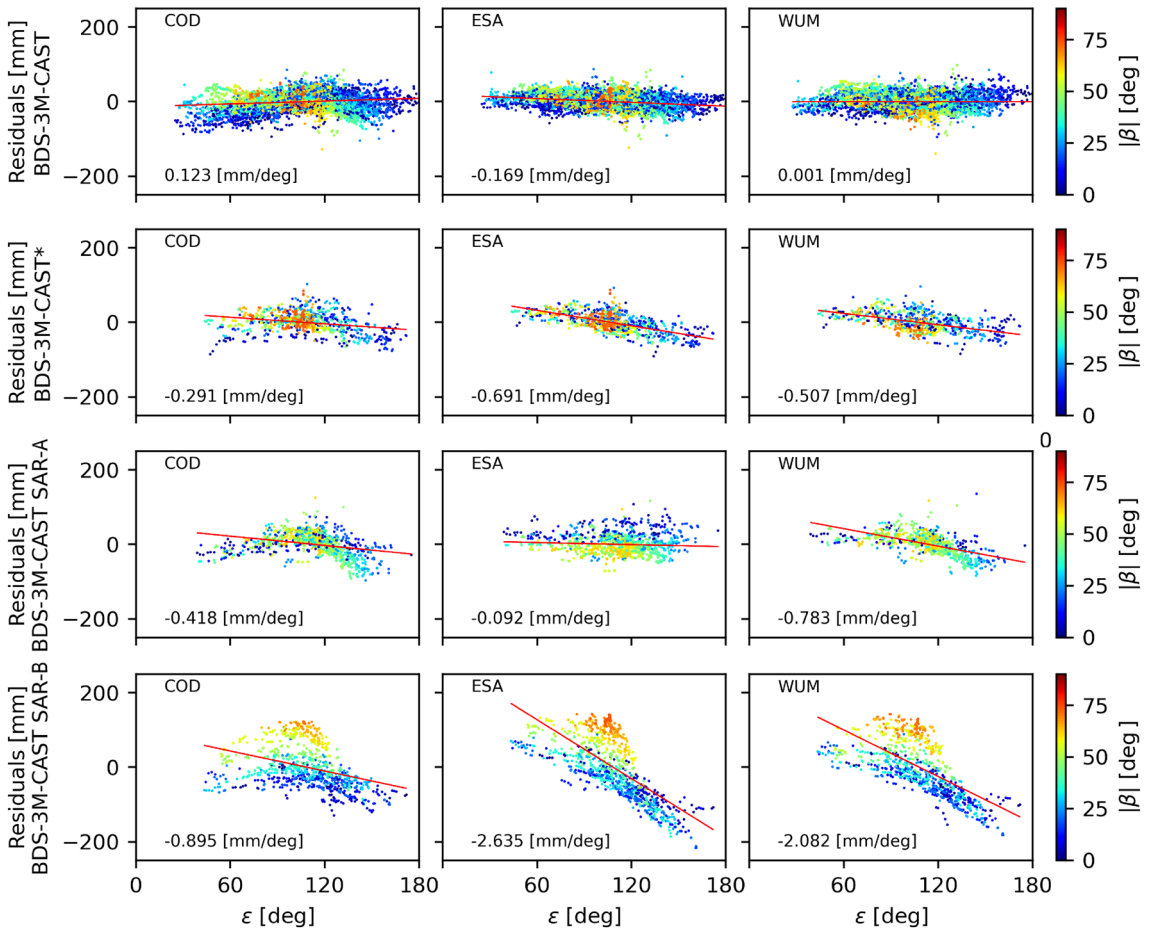

Fig. 11 SLR residuals as a function of satellite elongation angle with respect to the Sun position based on the individual AC solutions for different subgroups within BDS-3 MEO satellites manufactured by CAST

0.1 mm/° for WUM and COD/ESA, respectively. A weak linear correlation of about 0.9 mm/° is also evident for the BDS-3M-CAST SAR-A orbit solutions provided by ESA. For all other subgroups, linear coefficients span between 0.3 and even 2.6 mm/° for BDS-3M-CAST* and BDS-3M-CAST SAR-B, respectively.

Figures 12, 13 correspond to Figs. 10, 11, respectively, with a focus on the BDS-SECM satellites. For the BDS-3 M-SECM-A satellites, a pattern of negative SLR residuals becomes apparent for Δu values around 180° and β angles exceeding 30°. It is worth noting that the SLR residuals for $|\beta| > 30°$ belong to the C25/C26 satellites within orbital plane C3. This pattern is exclusive to this subgroup, as none of the other BDS-3-SECM satellites (located on plane C1) exhibits such geometry. As a result, this orbit modeling issue may be specific to these satellites and not affect the entire group. The pattern with negative SLR residuals for $|\beta| > 30°$ and $\Delta u = 180°$ is more pronounced in WUM products compared to ESA and COD solutions. Similarly, for BDS-3M-SECM-A* satellites, the patterns are consistent across solutions, showing more positive SLR residuals for Δu values near 90°/270° and negative values for Δu values near 180°. The extent of this pattern is most noticeable in COD and WUM solutions, whereas the spread of SLR residuals is smallest for ESA orbits.

Lastly, the SLR signatures visible for BDS-3M-SECM-B satellites point rather to an error in the LRA offset provided by CSNO than orbit modeling issue. It is challenging to identify any discernible patterns, and the SLR residuals resemble more of a noise pattern with a STD of around 200 mm, which can be explained by an offset in the X-Y LRA coordinates exceeding 1 m.

Figure 13 illustrates that the BDS-3M-SECM-A satellites display the least pronounced linear correlation between SLR residuals and the elongation angle, with values ranging from 0.03 to around 0.1 mm/° for WUM and COD/ESA, respectively. Furthermore, a subtle linear correlation of approximately 0.12 mm/° is evident in the BDS-3M-SECM-A* orbit solutions provided by ESA. Among the other subgroups, the linear coefficients encompass a range of 0.2 to even

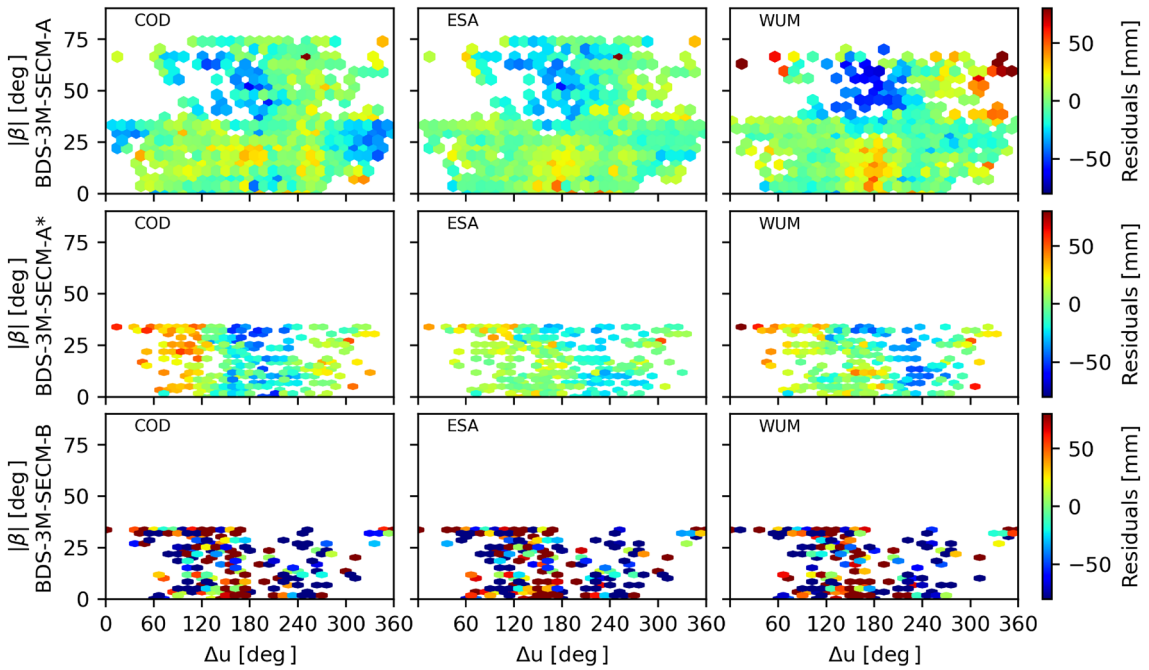

Fig. 12 SLR residuals as a function of the Sun elevation angle above the orbital plane (absolute value of β) and the satellite argument of latitude with respect to the latitude of the Sun (Δu) based on the individual AC solutions for different subgroups within BDS-3 MEO satellites manufactured by CAST

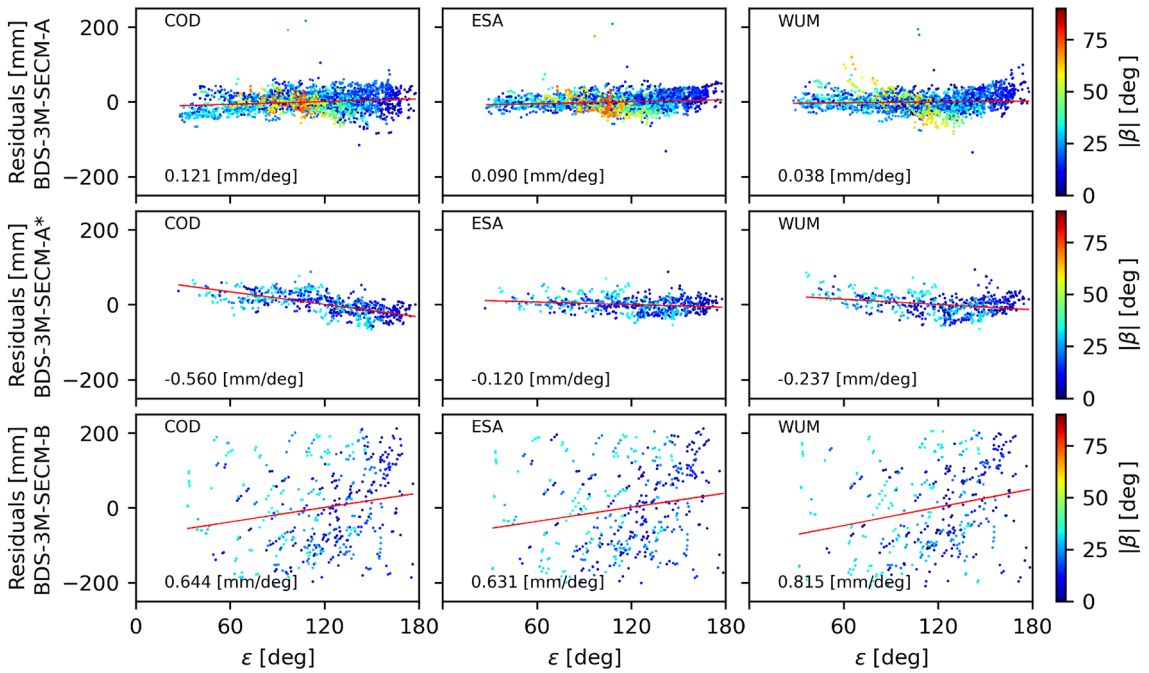

Fig. 13 SLR residuals as a function of satellite elongation angle with respect to the Sun position based on the individual AC solutions for different subgroups within BDS-3 MEO satellites manufactured by CAST

0.8 mm/° for BDS-3M-SECM-A* and BDS-3M-SECM-B, respectively.

Conclusions

In January 2023, ILRS agreed to commence tracking an additional set of 20 BDS-3 MEO satellites within the broader ILRS general pool, resulting in a significant increase from the previous tracking of only four satellites. Despite the incorporation of advanced GNSS components and technological solutions within BDS satellites, the acquisition of SLR tracking data has become a crucial factor in better understanding and addressing orbit modeling challenges. Enhanced orbit modeling is essential for integrating BDS into future terrestrial reference frame realizations, facilitating the determination of global geodetic parameters.

In this study, we provide a summary of the initial six-month tracking phase involving 24 BDS-3 MEO satellites. The results highlight the successful fulfillment of the ILRS network's request to track the entire BDS-3 constellation. Over the six-month period, around 1300 observations were collected for high-priority BDS-3 satellites, while approximately 450 observations were performed for low-priority satellites. Interestingly, a comparison of the number of normal points for BDS-3 and Galileo satellites reveals that for the non-ILRS priority satellites, the stations provided nearly twice as many observations for Galileo satellites compared to BDS-3 satellites. Notably, the bulk of laser observations for BDS-3 MEO satellites originated from only five out of the 24 active laser stations: 7237 (Changchun, 17%), 7819 (Beijing, 13%), 7821 (Shanghai, 11%), 7090 (Yarragadee, 11%), and 7827 (Wettzell, 7%), resulting in an uneven distribution of observational coverage globally, which is essential mainly for SLR-based orbit determination (Bury et al. 2019b). This station-dependent performance of the ILRS network has been a long-debated topic (Pearlman et al. 2019). Noting, in addition, the differences between the contribution of the individual stations to the observations of the constellations in question, it would be worthwhile to access, under simulated conditions, the impact of the distribution and the number of observations provided by the individual stations on the results of the validation of the orbits.

The efficacy of SLR tracking relies on the availability of orbit predictions. New BDS-3 orbit prediction files are typically released at intervals of about three days, occasionally with longer gaps of 5 to 10 days. By the 5th day of prediction, the 95th percentile position error extends to 35 m. A comparison of the number of observations with the quality of the prediction showed that the existing prediction quality offered by SHA is sufficient for the ILRS purposes. As of March 2023, due to the suspension of orbit prediction provision for the beidou3m7 (C27) and m8 (C28) satellites, the ILRS network observes 22 BDS-3 satellites instead of the full 24. This, however, may change if other sources start providing predictions for these satellites.

SLR validation of individual satellites has revealed that the BDS-3 MEO constellation comprises more satellite groups than initially documented in the official metadata files distributed by BDS system operators (CSNO 2019a, b). Additionally, the new SLR data have assisted in identifying issues with orbit modeling, particularly for satellites where modeling is challenging due to uncertainties in the macro models developed thus far.

The mean offset of SLR residuals for different individual satellites ranges from −50 to 50 mm. In addition to the officially defined satellite groups such as BDS-3M-CAST, BDS-3 M-SECM-A, and BDS-3M-SECM-B, four additional pairs of satellites with different SLR residual characteristics can be identified: C32/C33 (BDS-3M-CAST SAR-A), C45/C46 (BDS-3M-CAST SAR-B), C36/C37 (BDS-3M-CAST*), and C34/C35 (BDS-3M-SECM-A*). The current orbit modeling approaches used by the ACs appear to work well for BDS-3M-CAST and BDS-3M-SECM-A satellites. Achieving a STD of SLR residuals at the level of 19–20 mm is comparable to the quality of state-of-the-art Galileo orbit solutions (Zajdel et al. 2023). However, this applies only to 14 out of the 24 satellites in the BDS-3 MEO constellation, i.e., C19-C24, C41/C42 (BDS-3M-CAST); C25/C26, C29/C30 (BDS-3M-SECM-A); and C34/C35 (BDS-3M-SECM-A*). Therefore, improving orbit modeling for the remaining satellites remains a challenge for the GNSS community. For 8 BDS-3 satellites, the quality of the orbits is noticeably inferior with a standard deviation of SLR residuals above 100 mm, i.e., C32/C33 (BDS-3M-CAST SAR-A), C45/C46 (BDS-3M-CAST SAR-B), C36/C37 (BDS-3M-CAST*), and C43/C44 (BDS-3M-SECM-B).

Continued support from the ILRS network and increased observations for satellites needing special attention are recommended to facilitate this task. Currently, ILRS recommends tracking C20/C21 (BDS-3M-CAST) and C29/C30 (BDS-3M-SECM-A), for which, as shown, ACs provide orbits of the best quality. It could be then beneficial to recommend more intensive tracking of one satellite per each individual group, e.g., C20 (BDS-3M-CAST), C29 (BDS-3M-SECM-A), C32 (BDS-3M-CAST SAR-A), C36 (BDS-3M-CAST*), C43 (BDS-3M-SECM-B), and C45 (BDS-3M-CAST SAR-B).

Acknowledgements We would like to thank all who contributed to the start of tracking all satellites of the BDS-3 MEO constellation through the ILRS network, especially, Prof. Michael Pearlman (ILRS), Prof. Toshimichi Otsubo (ILRS), Claudia Cristina Carabajal (ILRS), and Dr. Oliver Montenbruck (IGS multi-GNSS Pilot Project). We thank Shanghai Observatory for providing orbit predictions and ILRS stations

for providing SLR observations. This work was funded by the National Science Centre, Poland (NCN), grant UMO-2019/35/B/ST10/00515 and Wroclaw University of Environmental and Life Sciences (UPWr) grant N060/0002/23. The APC is financed by Wrocław University of Environmental and Life Sciences (UPWr).

Author contributions RZ was responsible for performing the SLR validation of the orbits and the assessment of the ILRS GNSS tracking performance. AN analyzed the quality of orbit predictions. RZ wrote the main manuscript text. All authors contributed to the scientific discussion of the proposed methods and the results. All authors contributed to the manuscript review.

Data availability The COD and WUM BDS-3 final orbits are available in the IGS MGEX repositories, e.g., https://cddis.nasa.gov/archive/gnss/products/mgex/. The ESA BDS-3 orbit products are distributed at the separate ESA database, i.e., http://navigation-office.esa.int/products/gnss-products/. The SLR normal point observation files and orbit predictions for laser stations normal point data were obtained through the online archives of the Crustal Dynamics Data Information System (CDDIS), NASA Goddard Space Flight Center, Greenbelt, MD, USA. https://cddis.nasa.gov/archive/slr/data/.

Declarations

Conflict of interest The authors declare no competing interests.

References

Altamimi Z, Rebischung P, Collilieux X, Métivier L, Chanard K (2023) ITRF2020: an augmented reference frame refining the modeling of nonlinear station motions. J Geod 97:47. https://doi.org/10.1007/s00190-023-01738-w

Arnold D, Meindl M, Beutler G, Dach R, Schaer S, Lutz S, Prange L, Sośnica K, Mervart L, Jäggi A (2015) CODE's new solar radiation pressure model for GNSS orbit determination. J Geod 89:775–791. https://doi.org/10.1007/s00190-015-0814-4

Bury G, Zajdel R, Sośnica K (2019a) Accounting for perturbing forces acting on Galileo using a box-wing model. GPS Solut 23:74. https://doi.org/10.1007/s10291-019-0860-0

Bury G, Sośnica K, Zajdel R (2019b) Multi-GNSS orbit determination using satellite laser ranging. J Geod 93:2447–2463. https://doi.org/10.1007/s00190-018-1143-1

Bury G, Sośnica K, Zajdel R, Strugarek D, Hugentobler U (2020a) Determination of precise Galileo orbits using combined GNSS and SLR observations. GPS Solut 25:11. https://doi.org/10.1007/s10291-020-01045-3

Bury G, Sośnica K, Zajdel R, Strugarek D (2020b) Toward the 1-cm Galileo orbits: challenges in modeling of perturbing forces. J Geod 94:16. https://doi.org/10.1007/s00190-020-01342-2

Bury G, Sośnica K, Zajdel R, Strugarek D, Hugentobler U (2021) Geodetic datum realization using SLR-GNSS co-location onboard Galileo and GLONASS. J Geophys Res Solid Earth. 126:e2021JB022211. https://doi.org/10.1029/2021JB022211

Bury G, Sośnica K, Zajdel R, Strugarek D (2022) GLONASS precise orbit determination with identification of malfunctioning spacecraft. GPS Solut. https://doi.org/10.1007/s10291-021-01221-z

Chen X, Ge M, Liu Y et al (2023) Adapting empirical solar radiation pressure model for BDS-3 medium Earth orbitsatellites. GPS Solut 27:183. https://doi.org/10.1007/s10291-023-01524-3

CSNO (2019a) Definitions and descriptions of BDS/GNSS satellite parameters for high precision application. http://www.beidou.gov.cn/yw/gfgg/ 201912/W020200323534413026471.doc. Accessed 1 May 2022,

CSNO (2019b) Satellite information of BDS, China Satellite Navigation Office. http://en.beidou.gov.cn/SYSTEMS/Officialdocument/201912/P0202 00103556125703019.rar. Accessed 1 May 2022,

Dach R, Sušnik A, Grahsl A, Villiger A, Schaer S, Arnold D, Prange L, Jäggi A (2019) Improving GLONASS orbit quality by re-estimating satellite antenna offsets. Adv Space Res 63:3835–3847. https://doi.org/10.1016/j.asr.2019.02.031

Dach R, Fridez P, Lutz S, Walser P (2015) Bernese GNSS software version 5.2. doi: https://doi.org/10.7892/boris.72297

Delva P, Altamimi Z, Blazquez A, Blossfeld M, Böhm J, Bonnefond P, Boy J-P, Bruinsma S, Bury G, Chatzinikos M, Couhert A, Courde C, Dach R, Dehant V, Dell'Agnello S, Elgered G, Enderle W, Exertier P, Glaser S, Haas R, Huang W, Hugentobler U, Jäggi A, Karatekin O, Lemoine FG, Le Poncin-Lafitte C, Lunz S, Männel B, Mercier F, Métivier L, Meyssignac B, Müller J, Nothnagel A, Perosanz F, Rietbroek R, Rothacher M, Schuh H, Sert H, Sosnica K, Testani P, Ventura-Traveset J, Wautelet G, Zajdel R (2023) GENESIS: co-location of geodetic techniques in space. Earth Planets Space 75:5. https://doi.org/10.1186/s40623-022-01752-w

Duan B, Hugentobler U, Selmke I, Marz S, Killian M, Rott M (2022) BeiDou satellite radiation force models for precise orbit determination and geodetic applications. IEEE Trans Aerosp Electron Syst. https://doi.org/10.1109/TAES.2021.3140018

Enderle W, Schoenemann E, Mayer V, Springer T (2023) ESOC MGNSS processing strategy. doi: http://dgnl7.esoc.esa.int/products/gnss-products/esm.pdf

GSA (2017) Galileo satellite metadata. https://www.gsc-europa.eu/support-to-developers/galileo-satellite-metadata. Accessed 25 Jun 2020

Guo J, Xu X, Zhao Q, Liu J (2016) Precise orbit determination for quad-constellation satellites at Wuhan University: strategy, result validation, and comparison. J Geod 90:143–159. https://doi.org/10.1007/s00190-015-0862-9

Hackel S, Steigenberger P, Hugentobler U, Uhlemann M, Montenbruck O (2015) Galileo orbit determination using combined GNSS and SLR observations. GPS Solut 19:15–25. https://doi.org/10.1007/s10291-013-0361-5

Huang C, Song S, He L, Chen Q, Jiao W, Zhou W, Jiao G, Zhao H, Yang Y (2023) Estimation of antenna phase center offsets for BDS-3 satellites with the metadata and receiver antenna calibrations. J Geod 97:57. https://doi.org/10.1007/s00190-023-01757-7

Johnston G, Riddell A, Hausler G (2017) The international GNSS service. In: Teunissen PJG, Montenbruck O (eds) Springer handbook of global navigation satellite systems. Springer International Publishing, Cham, pp 967–982 (ISBN: 978-3-319-42928-1)

Li X, Yuan Y, Zhu Y, Jiao W, Bian L, Li X, Zhang K (2020) Improving BDS-3 precise orbit determination for medium earth orbit satellites. GPS Solut 24:53. https://doi.org/10.1007/s10291-020-0967-3

Li G, Guo S, He Z, Gao Y, Li W (2021) BDS-3 SAR service and initial performance. GPS Solut 25:134. https://doi.org/10.1007/s10291-021-01170-7

Lin X, Baojun L, Yingchun L, Sujie X, Tao B (2018) Satellite geometry and attitude mode of BDS-3 MEO satellites developed by SECM. pp 1268–1289.In: Proceedings of the 31st international technical meeting of the satellite division of the institute of navigation (ION GNSS+ 2018), Miami, Florida, pp 1268–1289. doi: https://doi.org/10.33012/2018.16118

Lyard FH, Allain DJ, Cancet M, Carrère L, Picot N (2021) FES2014 global ocean tide atlas: design and performance. Ocean Sci 17:615–649. https://doi.org/10.5194/os-17-615-2021

Montenbruck O, Steigenberger P, Prange L, Deng Z, Zhao Q, Perosanz F, Romero I, Noll C, Stürze A, Weber G, Schmid R, MacLeod K, Schaer S (2017) The multi-GNSS experiment (MGEX) of the international GNSS service (IGS)—achievements, prospects and challenges. Adv Space Res 59:1671–1697. https://doi.org/10.1016/j.asr.2017.01.011

Najder J, Sośnica K (2021) Quality of orbit predictions for satellites tracked by SLR stations. Remote Sens 13:1377. https://doi.org/10.3390/rs13071377

Noll CE (2010) The crustal dynamics data information system: a resource to support scientific analysis using space geodesy. Adv Space Res 45:1421–1440. https://doi.org/10.1016/j.asr.2010.01.018

Nowak A, Zajdel R, Sośnica K (2023) Optimization of orbit prediction strategies for GNSS satellites. Acta Astronaut 209:132–145. https://doi.org/10.1016/j.actaastro.2023.04.040

Pavlis EC (1995) Comparison of GPS S/C orbits determined from GPS and SLR tracking data. Adv Space Res 16:55–58. https://doi.org/10.1016/0273-1177(95)98780-r

Pearlman MR, Noll CE, Pavlis EC, Lemoine FG, Combrink L, Degnan JJ, Kirchner G, Schreiber U (2019) The ILRS: approaching 20 years and planning for the future. J Geod 93:2161–2180. https://doi.org/10.1007/s00190-019-01241-1

Petit G, Luzum B (2010) IERS—IERS Conventions (2010). Verlag des Bundesamts für Kartographie und Geodäsie, Frankfurt am Main. https://iers-conventions.obspm.fr/content/tn36.pdf

Prange L, Villiger A, Sidorov D, Schaer S, Beutler G, Dach R, Jäggi A (2020) Overview of CODE's MGEX solution with the focus on Galileo. Adv Space Res. https://doi.org/10.1016/j.asr.2020.04.038

Rodríguez J, Appleby G, Otsubo T (2019) Upgraded modelling for the determination of centre of mass corrections of geodetic SLR satellites: impact on key parameters of the terrestrial reference frame. J Geod 93:2553–2568. https://doi.org/10.1007/s00190-019-01315-0

Shi J, Ouyang C, Huang Y, Peng W (2020) Assessment of BDS-3 global positioning service: ephemeris, SPP, PPP, RTK, and new signal. GPS Solut 24:81. https://doi.org/10.1007/s10291-020-00995-y

SLRF2020 (2023) SLRF2020 product. Greenbelt MD USA NASA Crustal Dyn Data Inf Syst. https://doi.org/10.5067/SLR/SLRF2020_001

Sośnica K, Thaller D, Dach R, Steigenberger P, Beutler G, Arnold D, Jäggi A (2015) Satellite laser ranging to GPS and GLONASS. J Geod 89:725–743. https://doi.org/10.1007/s00190-015-0810-8

Sośnica K, Bury G, Zajdel R (2018) Contribution of multi-GNSS constellation to SLR-derived terrestrial reference frame. Geophys Res Lett 45:2339–2348. https://doi.org/10.1002/2017GL076850

Sośnica K, Bury G, Zajdel R, Strugarek D, Drożdżewski M, Kazmierski K (2019) Estimating global geodetic parameters using SLR observations to Galileo, GLONASS, BeiDou, GPS, and QZSS. Earth Planets Space 71:20. https://doi.org/10.1186/s40623-019-1000-3

Sośnica K, Zajdel R, Bury G, Bosy J, Moore M, Masoumi S (2020) Quality assessment of experimental IGS multi-GNSS combined orbits. GPS Solut 24:54. https://doi.org/10.1007/s10291-020-0965-5

Springer TA, Beutler G, Rothacher M (1999) A new solar radiation pressure model for GPS. Adv Space Res 23:673–676. https://doi.org/10.1016/s0273-1177(99)00158-1

Steigenberger P, Montenbruck O (2023) Consistency of Galileo satellite antenna phase center offsets. J Geod 97:58. https://doi.org/10.1007/s00190-023-01750-0

Steigenberger P, Montenbruck O, Hugentobler U (2015) GIOVE-B solar radiation pressure modeling for precise orbit determination. Adv Space Res 55:1422–1431. https://doi.org/10.1016/j.asr.2014.12.009

Steigenberger P, Deng Z, Guo J, Prange L, Song S, Montenbruck O (2023) BeiDou-3 orbit and clock quality of the IGS multi-GNSS pilot project. Adv Space Res 71:355–368. https://doi.org/10.1016/j.asr.2022.08.058

Steigenberger P, Montenbruck O (2022) IGS satellite metadata file description. Access: https://files.igs.org/pub/station/general/igs_satellite_metadata.snx

Steindorfer MA, Kirchner G, Koidl F, Wang P, Wirnsberger H, Schoenemann E, Gonzalez F (2019) Attitude determination of Galileo satellites using high-resolution kHz SLR. J Geod 93:1845–1851. https://doi.org/10.1007/s00190-019-01284-4

Strugarek D, Sośnica K, Arnold D, Jäggi A, Zajdel R, Bury G (2021) Determination of SLR station coordinates based on LEO, LARES, LAGEOS, and galileo satellites. Earth Planets Space 73:87. https://doi.org/10.1186/s40623-021-01397-1

Thaller D, Dach R, Seitz M, Beutler G, Mareyen M, Richter B (2011) Combination of GNSS and SLR observations using satellite co-locations. J Geod 85:257–272. https://doi.org/10.1007/s00190-010-0433-z

Wang C (2019) Solar radiation pressure modelling for BeiDou navigation satellites. Ph.D. Dissertation, GNSS Research Center, Wuhan University, Wuhan, China, 2019

Xie J, Kang C (2021) Engineering innovation and the development of the BDS-3 navigation constellation. Engineering 7:558–563. https://doi.org/10.1016/j.eng.2021.04.002

Xu X, Wang X, Liu J, Zhao Q (2019) Characteristics of BD3 global service satellites: POD, open service signal and atomic clock performance. Remote Sens 11:1559. https://doi.org/10.3390/rs11131559

Yan X, Liu C, Huang G, Zhang Q, Wang L, Qin Z, Xie S (2019) A priori solar radiation pressure model for BeiDou-3 MEO satellites. Remote Sens. https://doi.org/10.3390/rs11131605

Yang Y, Liu L, Li J, Yang Y, Zhang T, Mao Y, Sun B, Ren X (2021) Featured services and performance of BDS-3. Sci Bull 66:2135–2143. https://doi.org/10.1016/j.scib.2021.06.013

Zajdel R, Sośnica K, Bury G (2017) A new online service for the validation of multi-GNSS orbits using SLR. Remote Sens 9:1049. https://doi.org/10.3390/rs9101049

Zajdel R, Steigenberger P, Montenbruck O (2022) On the potential contribution of BeiDou-3 to the realization of the terrestrial reference frame scale. GPS Solut 26:109. https://doi.org/10.1007/s10291-022-01298-0

Zajdel R, Masoumi S, Sośnica K, Gałdyn F, Strugarek D, Bury G (2023) Combination and SLR validation of IGS Repro3 orbits for ITRF2020. J Geod 97(10):87. https://doi.org/10.1007/s00190-023-01777-3

Zhang Z-P, Zhang H-F, Chen W-Z, Li P, Meng W-D, Wang Y-M, Wang J, Hu W, Yang F-M (2014) Design and performances of laser retro-reflector arrays for Beidou navigation satellites and SLR observations. Adv Space Res 54:811–817. https://doi.org/10.1016/j.asr.2013.12.025

Zhao Q, Guo J, Wang C, Lyu Y, Xu X, Yang C, Li J (2022) Precise orbit determination for BDS satellites. Satell Navig 3:2. https://doi.org/10.1186/s43020-021-00062-y

Radosław Zajdel received a Ph.D. degree in Satellite Geodesy from Wroclaw University of Environmental and Life Sciences (UPWr) in 2021. His research interests include precise orbit determination of GNSS satellites and determining global geodetic parameters from multi-GNSS solutions.

Adrian Nowak graduated from the Faculty of Environmental Engineering and Geodesy at the Wroclaw University of Environmental and Life Sciences (UPWr), Poland, with a Master of Science degree in Geoinformatics in 2022. He specializes in GNSS satellite orbit predictions and determination of low-degree gravity field coefficients based on inverse GNSS methods.

Krzysztof Sośnica graduated from the University of Bern, Switzerland, in 2014, obtaining a Ph.D. degree in Physics. His activities include precise orbit determination of GNSS and geodetic satellites, Earth's gravity field recovery, and the enhancement of the consistency between GNSS and SLR solutions.